High-throughput sizing, counting, and elemental analysis of anisotropic multimetallic nanoparticles with single-particle inductively-coupled plasma mass spectrometry

Cedric David Koolen[a,b], Laura Torrent[c], Ayush Agarwal[c,d], Olga Meili-Borovinskaya[e], Natalia Gasilova[f], Mo Li[a,b], Wen Luo[g]*, Andreas Züttel[a,b]

[a]Laboratory of Materials for Renewable Energy (LMER), Institute of Chemical Sciences and Engineering (ISIC), Basic Science Faculty (SB), École polytechnique fédérale de Lausanne (EPFL) Valais/Wallis, Energypolis, Sion, 1951, Switzerland.

[b]Empa Materials Science & Technology, Dübendorf, 8600, Switzerland.

[c]Bioenergy and Catalysis Laboratory (LBK), Energy and Environment Research Division (ENE), Paul Scherrer Institute (PSI), Villigen, 5232, Switzerland.

[d]School of Architecture, Civil and Environmental Engineering (ENAC IIE GR-LUD), École Polytechnique Fédérale de Lausanne (EPFL), Lausanne, 1035, Switzerland

[e]TOFWERK AG, Thun, 3645, Switzerland.

[f]Mass Spectrometry and Elemental Analysis Platform (MSEAP), Institute of Chemical Sciences and Engineering (ISIC), Basic Science Faculty (SB), École Polytechnique Fédérale de Lausanne (EPFL) Valais/Wallis, Energypolis, Sion, 1951, Switzerland.

[g]School of Environmental and Chemical Engineering, Shanghai University, Shanghai, 200444, China.

*Corresponding author: wenluo@shu.edu.cn

Abstract

Nanoparticles (NPs) have wide applications in physical and chemical processes, and their individual properties (e.g., shape, size, and composition) and ensemble properties (e.g., distribution and homogeneity) can significantly affect the performance. However, the extrapolation of information from a single particle to the ensemble remains a challenge due to the lack of suitable techniques. Herein, we report a high-throughput single-particle inductively-coupled plasma mass spectrometry (SP-ICP-MS) based protocol to simultaneously determine the size, count, and elemental make-up of several thousands of (an)isotropic NPs independent of composition, size, shape, and dispersing medium with atomistic precision in a matter of minutes. By introducing highly diluted nebulized aqueous dispersions of NPs directly into the plasma torch of an ICP-MS instrument, individual NPs are atomized and ionized, resulting in ion plumes that can be registered by the mass analyzer (typically quadrupole, sector-field, or

time-of-flight tube). Our proposed protocol includes a phase transfer step for NPs synthesized in organic media, which are otherwise incompatible with ICP-MS instruments, and a modeling tool that extends the measurement of particle morphologies beyond spherical to include cubes, truncated octahedra, and tetrahedra, exemplified by anisotropic Cu NPs. Finally, we demonstrate the versatility of our method by studying the doping of bulk-dilute (<1 at. %) CuAg nanosurface alloys as well as the ease with which ensemble composition distributions of multimetallic NPs (i.e., CuPd and CuPdAg) can be obtained providing different insights in the chemistry of nanomaterials. We believe our combined protocol could deepen the understanding of macroscopic phenomena involving nanoscale structures by bringing about a statistics renaissance in research areas including, amongst others, materials science, materials chemistry, (nano)physics, (nano)photonics, catalysis, and electrochemistry.

Keywords

Nanoparticle, Single-particle ICP-MS, multimetallic, size, shape, composition, protocol

1. Introduction

The size and composition of nanoparticles (NPs) have shown to play an important role in a variety of physical and chemical processes, including light-matter interactions, magnetism, catalysis, etc. [1,2,3,4,5,6] To determine structure-property relations for such phenomena, the size and composition of the NP must be accurately and precisely described. Advancements in electron tomography using aberration-corrected microscopes have allowed for an exact 3D description of NPs with each individual atom accounted for.[7] However, at least eight orders of magnitude separate a single particle from its bulk powder. Therefore, the sample space that can reasonably be attained with high resolution electron microscopes (EM) is too low for statistically sound extrapolation to the bulk. An information gap immerges.[8,9]

More crudely but with better statistics, NPs can be sized through the production of low resolution EM images and subsequent automated edge-length analysis.[10,11] Several commercial and open-source image processing software exist that can be of aid herein.[12,13,8] However, exact determination of atomicity using such approaches is impossible as the resolution required lies outside the information limit. Further, the success of automated sizing is often frustrated by tedious sample preparation steps and the large quantities of micrographs needed for reasonable statistics.[8,9] In the present study, we propose the use of a methodology complementary to EM that allows to determine atomicity, composition, size, and number concentration of inorganic NP dispersions independent of element and shape with ensemble-representative statistics in a

single experiment, based on single-particle inductively-coupled plasma mass spectrometry (SP-ICP-MS).[14,15,16,17,18]
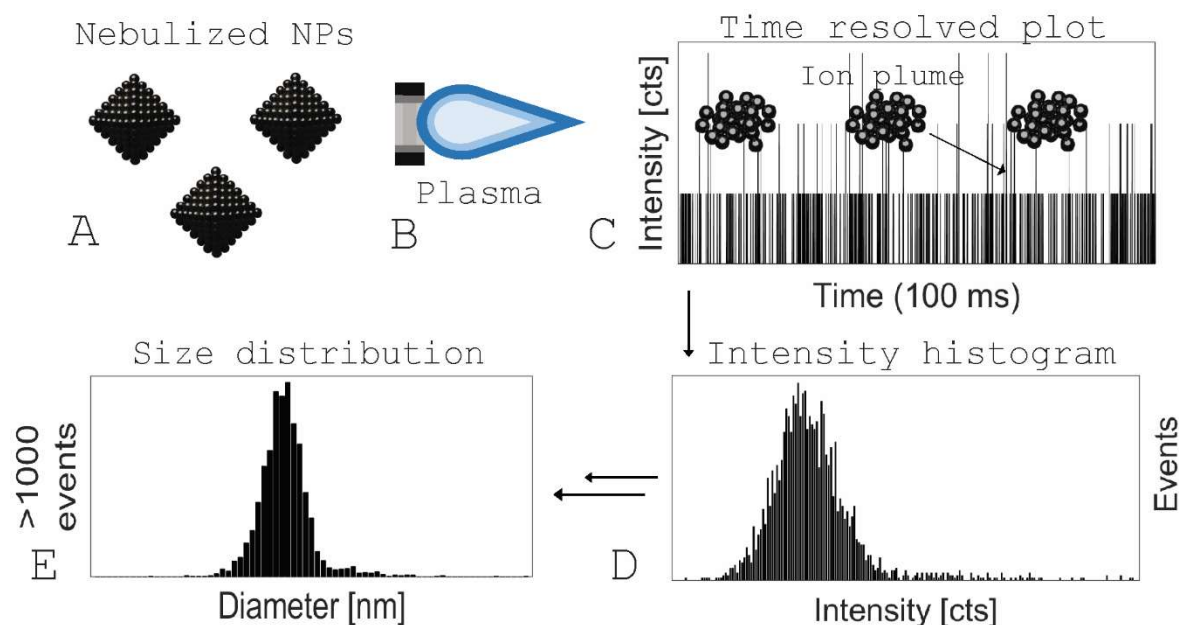

Figure 1. Schematic diagram of the general approach for obtaining size distribution of NP dispersions using SP-ICP-MS. (A) Nebulized NPs formed after nebulization of the sample dispersions. (B) Plasma torch of the ICP-MS instrument used for the desolvation, vaporization, atomization, and ionization of the particles present in the aerosol. (C) SP-ICP-MS raw data containing both background signal (e.g., dissolved ions) and particle events (ion plumes). A snapshot of 100 ms is depicted for representation. (D) Histogram of the raw data obtained via a sorting algorithm after background subtraction equating the intensity to the number of observations (events). (E) Final solution of SP-ICP-MS data processing pipeline, e.g., size distributions.

ICP-MS is routinely used to determine the concentration of elements in their ionic form. In the framework of nanomaterials, this entails the digestion of particulate matter using strong acids such as concentrated nitric acid (HNO_3), hydrochloric acid (HCl), or aqua regia yielding dissolved ionic solutions of the respective materials. The MS determines the ion intensities of a defined mass to charge ratio for each of the analytes and correlates it to the absolute concentration based on the external calibration curve prepared using standard solutions of the analytes at known concentrations.[19] Such an approach allows for the determination of average elemental make-up, synthesis yields, dispersion concentrations etc., but is insensitive to the homogeneity of the ensemble. For an ICP-MS instrument with a quadrupole mass analyzer, an intensity reading is acquired every defined time interval, known as dwell time or integration time, and averaged over the total acquisition time. Instead, in SP-ICP-MS, undigested NP

dispersions are nebulized and introduced to the plasma torch directly, after which the individual particles become desolvated, vaporized, atomized and ionized, and arrive at the mass analyzer as discrete ion packages, or ion plumes, retaining the information of the elemental make-up of each individual particle (**Figures 1A, B**).[20] Intensity spikes above the background herald the arrival of an ion plume or particle event at the detector. This is distinctively different from dissolved ion intensities, or background signal, which remain constant. To distinguish between these discrete particle events and the dissolved ions, dwell times much shorter than in conventional ICP-MS are needed (µs to ms). Each individual acquisition of the intensity read-out is then plotted against the acquisition time representing the SP-ICP-MS raw data (**Figure 1C**). A series of steps (**Figure 1D**) have to be executed before raw SP-ICP-MS data can be transformed into a meaningful data-set such as a NP size distribution (**Figure 1E**).[14,16]

Traditionally, SP-ICP-MS has been used to determine particle number concentrations and size distributions of undefined, crude dispersions relevant to environmental research, health and/or food sciences, limited to metal oxides and noble metals such as Au, Ag, and Pt.[15,17,20,21,22,23,24,25,26] Recently, some more complex analytes (e.g., TiNbCN and AuAg) have been studied as well albeit of undefined morphology or isotropic in nature.[27, 28] Moreover, due to the incompatibility of ICP-MS with organic solvents, samples analyzed are produced or dispersible in water alone. Herein, we show the capabilities of SP-ICP-MS to determine the size, count and composition of transition metal (an)isotropic (multi)metallic NPs of well-defined size and shape, including but not limited to spheres, cubes, truncated octahedra and tetrahedra, synthesized in organic media using in-house developed syntheses (**Figure 2**). We further demonstrate that the high sensitivity of the quadrupole mass analyzer allows to quantify the atomicity of bulk-dilute (<1 at. %) anisotropic CuAg nanosurface alloys (NSA), corroborated with X-ray photoelectron spectroscopy (XPS), offering a roadmap for the study of NP doping with reliable statistics using SP-ICP-MS. Finally, by extending upon our in-house developed syntheses, we produce CuPd and CuPdAg cubic multimetallic NPs and use a time-of-flight (TOF) ICP-MS to show that the composition of NP ensembles can be studied with ease. We further verify these results with scanning transmission electron microscopy energy dispersive X-ray spectroscopy (STEM-EDX). We aim at providing a method to the reader to quantify (an)isotropic inorganic NP dispersions complementary to EM. We believe that this method can also be applied to a variety of materials, including semiconductors (e.g., CdSe, $CsPbBr_3$, InP, etc.), upconversion nanocrystals (e.g., $NaYF_4$, $NaGdF_4$, $NaLuF_4$, etc.), metal oxide (e.g., Al_2O_3, TiO_2, ZnO_2 etc.), metal organic frameworks (e.g., ZIF-8, HKUST-1, UiO-

66, etc.) and finally, metals and alloys (e.g., Mn, Co, Ni etc.). Therefore, a complete description of the instrument calibration and data processing pipeline is provided in the following section.
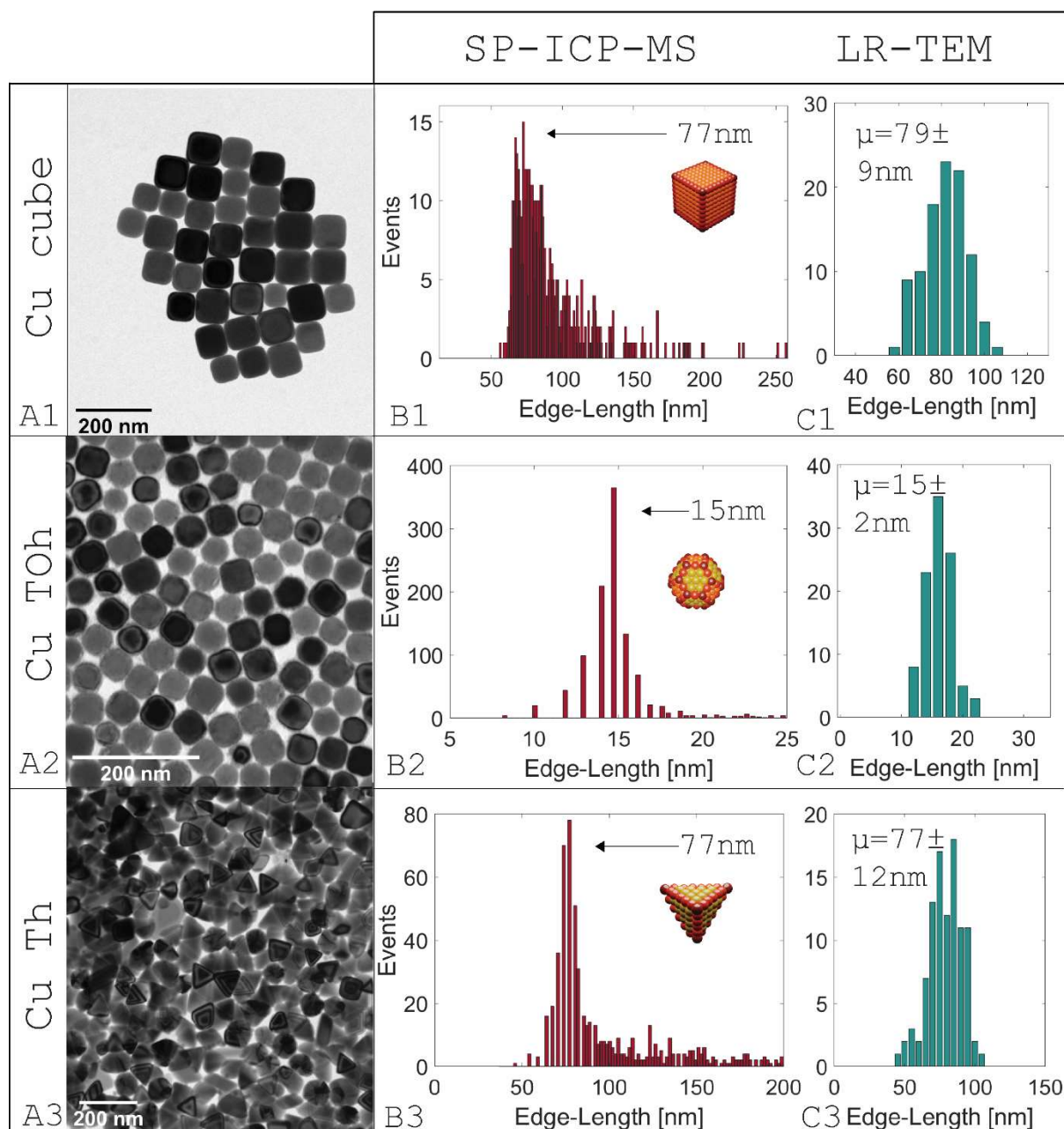

Figure 2. (A1-A3) Low resolution transmission electron microscopy (LR-TEM) micrographs of cubic (C), truncated octahedral (TOh), and tetrahedral (Th) Cu NPs synthesized using a phosphine-derivative mediated wet-chemical procedure. (B1-B3) Size distributions of the C-, TOh- and Th-Cu NPs obtained using SP-ICP-MS. The particle most frequently observed has an edge-length of: 77, 15 and 77 nm, respectively. Edge-length is defined as the center-to-center distance between two corner atoms of a particle (depicted in deep red in the ball models in the inset). The total number of particles observed in a single experiment was as high as 1100 for a measurement of 100 s duration with a dwell time of 50 μs. Excellent agreement exists between the SP-ICP-MS and LR-TEM (C1-C3) measurements.

Aggregates in the sample that are missed by the LR-TEM can be observed (events at the far end of the distributions in (B1-B3), giving a more complete picture of the ensemble. (C1-C3) Size distributions of 100 C-, TOh- and Th-Cu NPs using particle counting of LR-TEM micrographs.

2. Instrument calibration and data processing

As described in the introduction, SP-ICP-MS raw data consist of a signal intensity as a function of time (**Figure 3A**). This includes a background/dissolved analyte signal and particle events evidenced by intensity spikes above the background. In order to extract all particle events, background subtraction has to be performed, which is achieved mathematically and iteratively (see **Methods**). All extracted particle events are then grouped and sorted based on their respective intensity values and reported as events-versus-intensity histograms (**Figure 3B**).[29] The total number of events is a direct measure of the number of particles that have reached the detector, which can be converted into a number concentration using Eq. 1:

$$N = \frac{f}{tQ\eta_t} \tag{1}$$

in which N is the NP number concentration (mL^{-1}), f the total number of events, t the total acquisition time (min), and Q the sample flow rate (mL min^{-1}), which can be estimated from the mass change of an arbitrary volume of water consumed by the instrument as a function of time. The dimensionless quantity η_t, known as the transport efficiency, is introduced to account for the fraction of particles originally introduced that can actually be detected and is generally <10%.[14,16] This is due to losses associated with the generation of the aerosol, which is instrument and size dependent.[30] Therefore, sets of known particle size and concentration are introduced and their observed number concentrations are determined (**Figure 3C**). Calibration can then be performed using Eq. 2:

$$N_{obs} = \frac{f}{Qt} = \eta_t N_{Theo} \tag{2}$$

in which N_{obs} is the observed particle number concentration and N_{Theo} the theoretical particle number concentration. Alternatively, calibration can also be performed based on the particle size but requires an additional external calibration step.[14,16] Often used calibrants are monodisperse isotropic Ag and Au NPs, which can be purchased from various sources and of which the latter is used presently (see **Methods, Figure S1** and **S2**). In theory, any set of well-defined, monodisperse particles with known characteristics can be used for the calibration. Ideally, one would use standard dispersions of the same element as well as the same matrix as

the analyte. However, commercial availability is limited. Therefore, we are working on sets of synthesized NP calibrants to match our analyte and determine its effect, if any, which is the subject of a later work.
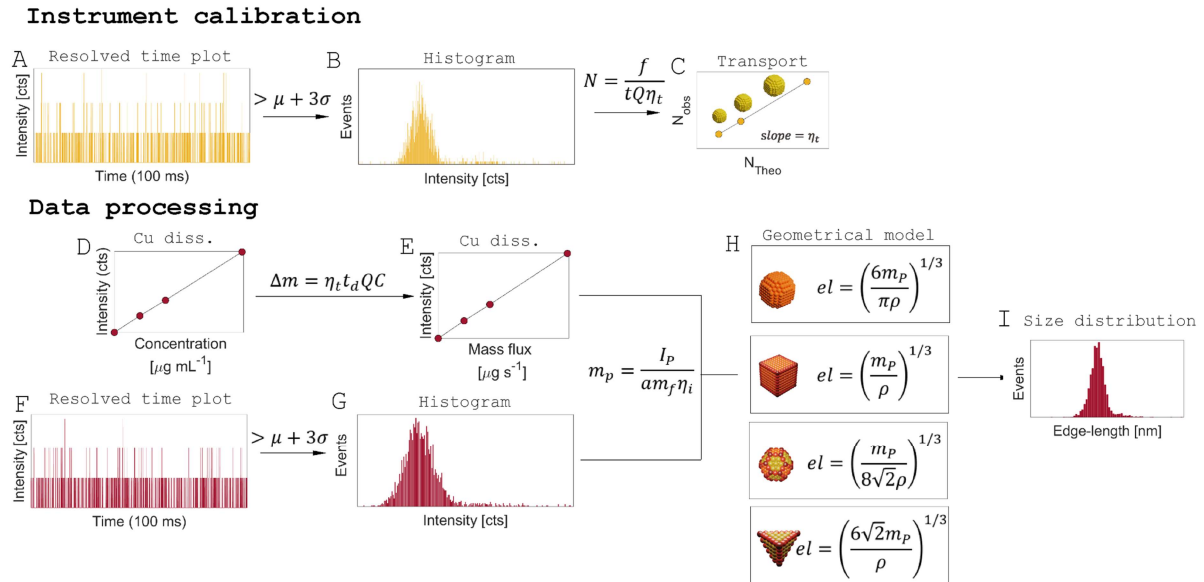
Instrument calibration

Figure 3. (A) Time resolved plot of the SP-ICP-MS raw data of a calibrant (yellow). Only 100 ms is depicted for clarity. (B) Intensity-versus-events histogram of a calibrant (yellow). (C) Transport efficiency (η_t) calibration curve of particle dispersions of known size and number concentration (in the present study Au NP (see **Methods, Figure S1** and **S2**). (D) Dissolved standard solutions calibration curve (Cu in the present study). (E) Converted µg s^{-1} calibration curve of the dissolved ion standards (Cu in the present study). (F) Time resolved plot of the SP-ICP-MS raw data of an analyte (red). (G) Intensity-versus-events histogram of an analyte (red). A snapshot of 100 ms is depicted for representation. (H) Various geometrical models to extract dimensional parameters such as edge-length including but not limited to spheres, cubes, truncated octahedra and tetrahedra. (I) Final solution of the SP-ICP-MS data processing pipeline representing a NP size distribution.

With the instrument calibrated and η_t obtained, one could directly measure the number concentration of a given unknown NP dispersion. However, in order to determine the mass of the particles counted, another calibration is required. As mentioned before, in ICP-MS, the dissolved analyte concentration of an unknown solution is determined by comparing its average intensity to the intensity measured of solutions of known concentrations. However, SP-ICP-MS intensities are detected at discrete intervals. Therefore, to relate such a discrete intensity to an ion plume mass, the average concentration of the calibration curve (µg mL^{-1}; **Figure 3D**)

needs to be converted into the amount of material detected at any given dwell time ($\mu g\ s^{-1}$; **Figure 3E**). This can be achieved according to Eq. 3:

$$\Delta m = \eta_t t_d Q C \tag{3}$$

in which t_d is the dwell time (or integration time) and C the dissolved ion concentration. The slope of the converted calibration curve (a) then relates the intensity of the ion plume (I_p) to the particle mass (m_P) through Eq. 4:

$$m_p = \frac{I_p}{a m_f \eta_i} \tag{4}$$

in which η_i is the ionization efficiency, the dimensionless parameter that allows for a correction factor for materials that ionize poorly. Partial ionization is strongly mass dependent both relative and absolute, and has been determined for Au to occur for particles >150 nm.[20,31] Further, partial ionization may also play a role for metal oxides for their generally high boiling points.[20,31] As the materials investigated in this study (i.e., Cu, CuAg, CuPd, and CuPdAg NPs) have lower melting points and ionization potentials than Au and are smaller than 150 nm in size, it is reasonable to assume an ionization efficiency of 100%. Another parameter m_f, the mass fraction, or the contribution of the element analyzed to the total particle mass, is introduced for modelling purposes. For example, only metal species in metal oxides can be detected by ICP-MS and this can be accounted for by a corresponding m_f value.

With the particle mass in hand, the events per intensity histogram of the analyte can be converted into a size distribution of a specific particle geometry by using a dimensional descriptor such as the edge-lengths (el). This includes but is not limited to spheres (Eq. 5), cubes (Eq. 6), truncated octahedra (Eq. 7), and tetrahedra (Eq. 8):

$$el_{Sph} = \left(\frac{6 m_p}{\pi \rho}\right)^{\frac{1}{3}} \tag{5}$$

$$el_{Cu} = \left(\frac{m_p}{\rho}\right)^{\frac{1}{3}} \tag{6}$$

$$el_{TOh} = \left(\frac{m_p}{8\sqrt{2}\rho}\right)^{\frac{1}{3}} \tag{7}$$

$$el_{Th} = \left(\frac{6\sqrt{2} m_p}{\rho}\right)^{\frac{1}{3}} \tag{8}$$

where ρ is the density.

3. Results and Discussion

3.1 NP concentration optimization

In order to have the most accurate measurement, it is adamant that each particle event can be distinguished from the background. If the ionic contribution to the signal is too high (e.g., a residual from the synthesis), NPs having intensities similar or below that of the dissolved analyte cannot be identified by the algorithm. However, since the intensity of each particle is fixed and the intensity of the dissolved analyte is concentration dependent, sample dilution can help detect the smaller particles in the ensemble as well (for particles above the limit of detection (LOD)).[32,33] To evaluate the effect of NP concentration on the results, in **Figure 4**, a suspension of 15 nm TOh-Cu NPs at a concentration of 10^5 mL^{-1} was analyzed by SP-ICP-MS as well as their 3- and 6-fold dilutions. The measured most frequent size was: 29 nm (**Figure 4A**, **Table S1**), 23 nm (**Figure 4B**, **Table S1**) and 15 nm (**Figure 4C**, **Table S1**), respectively. The latter one portrays the complete distribution whereas for the former two only a portion of the ensemble can be observed. This shows the dissolved analyte concentration cap. Above it, the background signal is too high to extract the full distribution. Diluting further, on other hand, will result in progressively lower numbers of events as less and less intervals will contain a particle event. Of course, this could be off-set by extending the measurement time but this is rather impractical: for every additional second measured, with $t_d = 50$ μs, 2×10^4 data points are added to the data file. Therefore, there exists an optimized dissolved analyte to particle concentration that yields good statistics with the least amount of data, but excludes the loss of information due to a too high ionic background. For the Cu NPs reported here and using the instrument settings as outlined in the **Methods** section, this optimal concentration lies between 10,000-20,000 mL^{-1}. However, this value can vary strongly between particles of different elements and depends on both the chemical nature of the NPs, their size, the instrument and its corresponding settings and finally the synthesis procedure used (e.g., for Au NPs of 30-100 nm used presently this value is ~50,000 mL^{-1} for $t_d = 50$ μs on a quadrupole based ICP-MS instrument).[34,29] Preparing dilution series as in **Figure 4** can be of tremendous value to calibrate a measurement when optimal number concentrations are unknown. It is worth noting the difference in events between **Figure 4A, 4B** and **4C**. When the dissolved analyte concentration is too high, only the tail of the distribution can be extracted resulting in a low number of events. Once the ionic background intensity falls below that of the smallest particle of the ensemble, the total number of events goes up by at least an order of magnitude. This change in NP events can be used as a handle to find the optimal concentration.
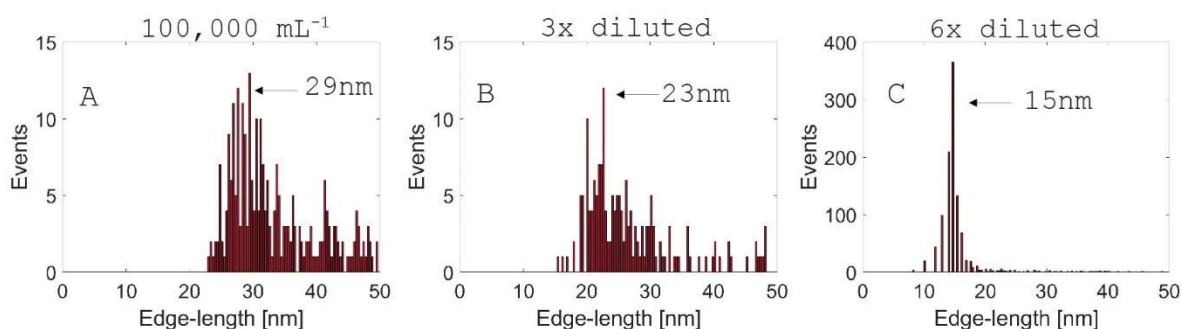
Figure 4. Size distributions of a dilution series of TOh-Cu NPs. (A) NP number concentration (N): 10^5 mL^{-1}, (B) NP number concentration (N): $1/3 \times 10^5$ mL^{-1}, (C) NP number concentration (N): $1/6 \times 10^5$ mL^{-1}. Shift of the average size, thus mass, to lower values. upon dilution highlights the significant effect of the dissolved analyte concentration on data quality. If the dissolved analyte concentration is too high, ion plumes derived from initial particles of intensities close to the dissolved analyte cannot be distinguished from the background. Optimization and calibration of N is instrumental to correct distribution determination. This feature perseveres even with an independent instrument calibration used (**Figure S3**). The gain in the number of events is evidence that all particle events can be extracted.

3.2 Reliability of the method

To determine the reliability of the technique to provide reproducible size distributions (as it is still one of the main means to show ensemble (in)homogeneity),[10,11] we prepared two dilution series of the same NPs (TOh-Cu, **Figures 4A-C** and **S3A1-C1**) but used independent standards for the instrument calibration of η_t (**Figures S1** and **S2**). By using the same mass s^{-1} calibration curve for both dilution series (**Figure S4**), we ensured that any changes to the size distribution that originated from inaccuracy in the determination of the η_t, which is expected to introduce the largest error,[14] are taken into account. When the particle concentration reaches its optimal value, a perfect match in the particle mass is obtained with the edge-length of the TOh-Cu NPs determined at 15 nm in both cases, independently of calibrant used (**Figures 4C** and **S3C1**). With a well-calibrated instrument, precise and accurate size distributions can be obtained reproducibly, independent of particle size and shape (for particles above the LOD) as equally agreeing results could be obtained for the Th-Cu NPs (**Figures S3A2-C3** and **S4**).

We further investigated the accuracy and precision of SP-ICP-MS to determine NP number concentrations as they are of interest to study colloidal stability, nanoparticle sintering and catalytically active surface area estimation, amongst others.[35,36,37,38] We prepared six independent dilutions of C-, TOh-, and Th-Cu NPs, based on a three-fold dilution series, and measured the particle concentrations (**Table S2**). With an uncertainty of the measurement of

only 4% (estimated through error propagation of the dilution series based on manufacturer reported uncertainties at 2%, **Table S2.2**), SP-ICP-MS allows for number concentration determinations with high precision. Further, it reveals a consistently lower particle concentration (~10%) than estimated based on LR-TEM particle counting. This is most likely a result of aggregates in the sample, however.

3.3 Applications

Beside the size and the particle number concentration, SP-ICP-MS can be used to quantify different elements within a particle ensemble.[40] Due to the short dwell times needed for SP-ICP-MS, TOF mass analyzers are required to obtain a full elemental spectrum in a single dwell/integration time.[18,20,41,42] Very recently, a SP-ICP-MS method has been established to simultaneously measure two elements by extending the signal duration through the introduction of a collision cell.[28] This limits the LOD, however. Alternatively, one may perform sequential spectral analysis.[20] Using a galvanic exchange reaction, we were able to synthesize anisotropic CuAg NSAs (C-CuAg, **Figure 5A1, A2** and TOh- and Th-CuAg **Figure S6**). With the Ag and Cu distributions obtained via SP-ICP-MS, followed by a subsequent subsurface based modelling step (**Figure S5**), we were able to determine the ensemble average surface composition of our anisotropic particles (**Figure 5C1-C2**). We deduce that 0.59 monolayer of Ag has been deposited in the case of the C-CuAg NSA. Further, we show that Ag at. ‰ is normally distributed around the mean (max. Ag 9 at. ‰, **Figure 5C2)**. Our method offers the same information as for dopant distributions that have been studied for bulk materials, e.g., n-type semiconductors.[43,44,45] We further confirmed these results with the good agreement of those obtained from XPS by comparing the estimated penetration-depth to the inelastic mean free path information depth (error <5%, **Figure S7** and **Table S3**).[46]
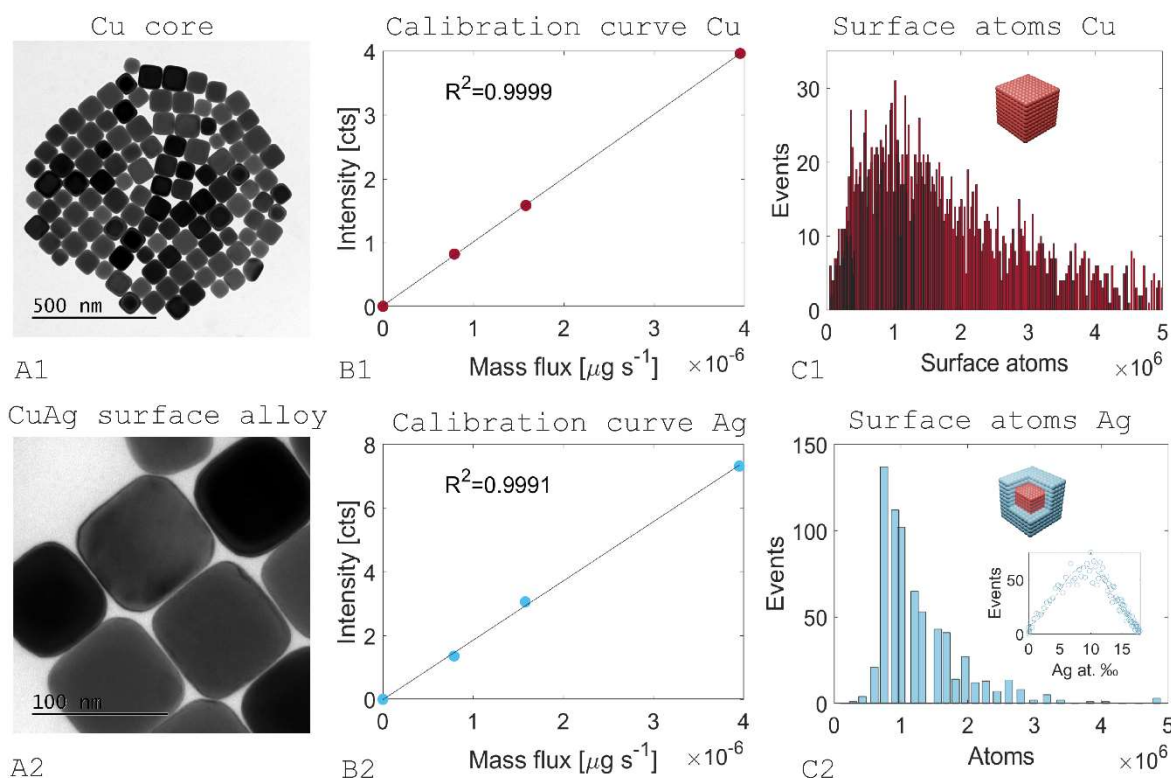
Figure 5. SP-ICP-MS as a method to characterize anisotropic NSAs.[39] The C-Cu NPs synthesized in the present study were coated with an ultrathin shell of Ag using a galvanic exchange reaction (see **Methods**). (A1-A2) LR-TEM micrograph of the Cu cubic core and the CuAg cubic NSA, respectively. (B1-B2) Cu and Ag mass flux calibration curve used to convert the intensity measured to the mass of the particle. (C1) Using a subsurface model (**Note S2**, **Figure S5**), the Cu particle mass distribution obtained with SP-ICP-MS can be converted into an ensemble distribution of surface atoms. (C2) Distribution of Ag atoms obtained via SP-ICP-MS. By taking the ensemble average, we deduce that 0.59 monolayer of Ag has been deposited. Inset shows the normally distributed doping concentration of Ag by superimposing the Cu and Ag spectra, respectively.

While sequential analysis suffices for simple bimetallic samples, experiment and data treatment quickly becomes tedious for more complex systems (e.g., high-entropy alloys[47]). Further, data treatment requires assumptions and preexisting knowledge of the sample, e.g., that each particle contains all elements. Therefore, we further extended upon our galvanic replacement reaction to produce next to C-CuAg NSAs, C-CuPd and C-CuPdAg anisotropic multimetallic NPs to show the capabilities of TOF mass analyzers to determine the elemental make-up of every *single* particle simultaneously and its advantage over quadrupole mass analyzers for, e.g., doping studies (**Figure 6**). As a benchmark, we first sized C-Cu NPs using SP-ICP-TOFMS to determine the reliability of the method and alternative calibration procedure using monodisperse microdroplets of element solutions, which showed an excellent match with LR-

TEM (**Figure S8**). Further, we confirmed the normal distribution of Ag in the C-CuAg NSA (**Figure 6C1**) and determined that in the case of CuPd, a positive skew ensured with an order larger Pd content (**Figure 6C2**). We invoke differences in standard reduction potentials of both metals to explain the difference in reactivity (+0.7996 and +0.915 V for Ag(I) and Pd(II), respectively). We could verify the presence of Ag and Pd in the respective bimetallic systems using STEM-EDX, which showed a core-shell like morphology for C-CuPd NPs, corroborating the higher average Pd content determined with SP-ICP-TOFMS (**Figure 6B1-B2**). Moreover, by reintroducing C-CuAg NSAs in the Pd-precursor reaction mixture, we were able to synthesize C-CuPdAg NPs as well (**Figure 6A3-C3**). Interestingly, it could be deduced that Ag had corroded instead of the expected Cu alone (+0.52 V, **Figure S9**). This can be explained by the more facile etching of Ag in the presence of Cl^- ions. Further scrutiny of the SP-ICP-TOFMS data pointed towards the presence of bimetallic AgPd NPs in the ensemble as well albeit of low occurrence. After reexamination of the sample with STEM-EDX, these particles could eventually be observed likewise (**Figure S10**). Finally, we show that using SP-ICP-TOFMS it is possible to distinguish bimetallic physical mixtures (CuAg + CuPd) from multimetallic NPs, which would not have been possible using a quadrupole mass analyzer (**Figure S11**). With the TOF instrument used presently, any ion within the range of 7-175 *m/z* can be observed simultaneously (**Table S4**).[48] This includes most of the elements of the periodic table. However, not all elements can be observed with equal sensitivity. For a list of elements that can be quantified with SP-ICP-TOFMS and their reported LODs if any, we direct the reader to the SI (**Table S5**).
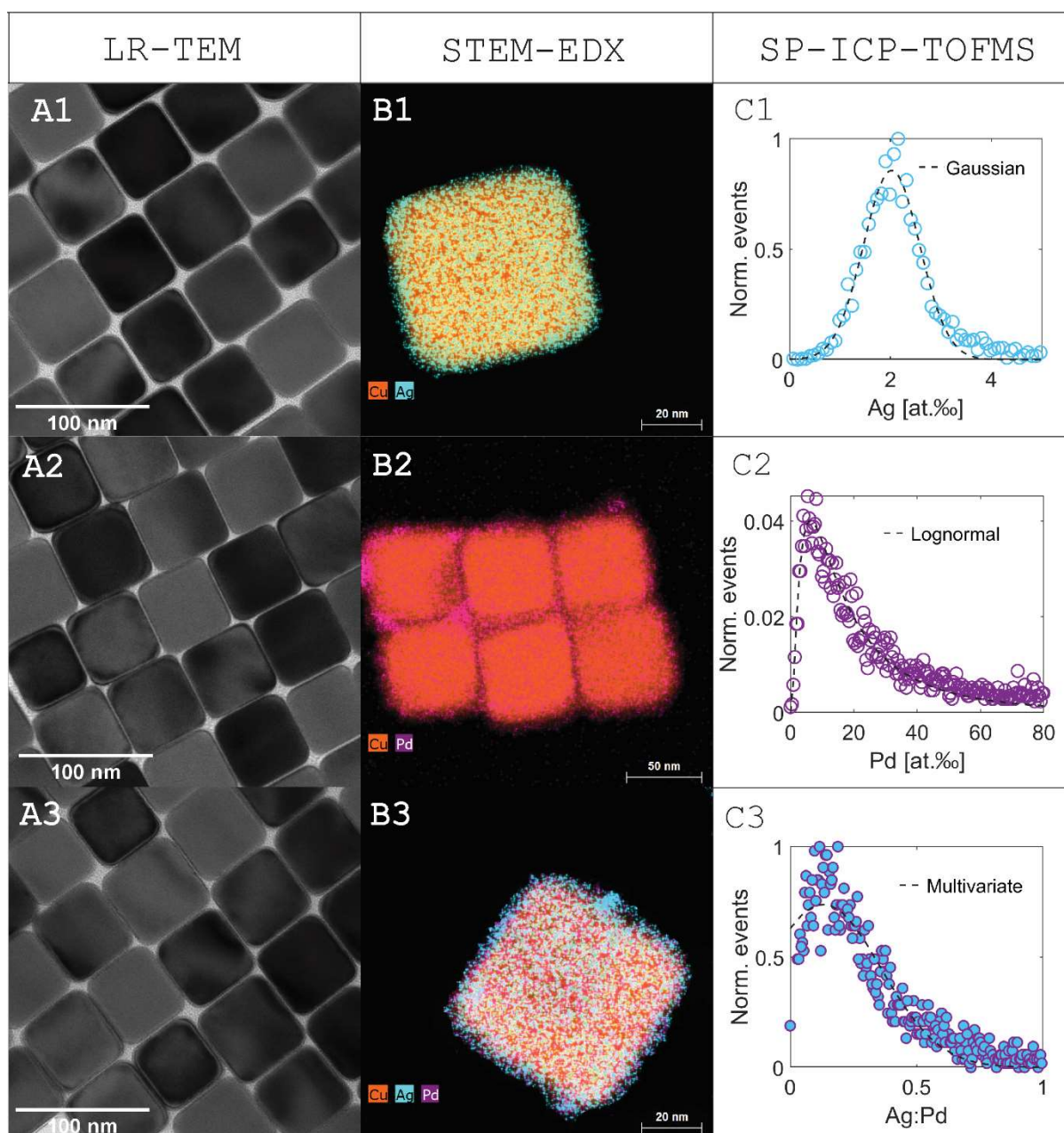
| LR-TEM | STEM-EDX | SP-ICP-TOFMS |

Figure 6. (A1-A3) TEM micrographs of the C-CuAg, C-CuPd, and C-CuPdAg multimetallic NPs, respectively. (B1-B3) STEM-EDX elemental maps of C-CuAg, C-CuPd, and C-CuPdAg NPs. (C1-C3) Normalized composition distributions of C-CuAg, C-CuPd, and C-CuPdAg multimetallic NPs obtained with a TOF mass analyzer. The C-CuAg and C-CuPdAg distributions were normalized by the number of events. The C-CuPd distribution was normalized so that the probability density function integral equaled to one. (C1) The C-CuAg distribution shows that Ag is normally distributed around the mean, corroborating the results obtained using the quadrupole (Gaussian fit: $R^2 = 0.9723$, see **Note S4**). The maximum lies at ~2.2 Ag at. ‰, a four-fold reduction with respect to the SP-ICP-MS determined composition distribution (**Figure 5C2**), which can be explained by the higher number concentration at a fixed mass loading (see **Figure S8** and **S12**). (C2) The C-CuPd is lognormally

distribution evidenced by the positive skew ($R^2 = 0.9816$, see **Note S4**. (C3) The C-CuPdAg distribution shows again a normal distribution ($R^2 = 0.9467$, see **Note S4**).

4. Conclusion

The high-throughput, element discriminative, dispersing media indiscriminate, size and shape independent NP dispersion quantification and characterization protocol offered presently, based on SP-ICP-MS, is a powerful tool that may help bring about a statistics renaissance in the nanomaterial's science world. With this approach, nanoscale structures relevant to bulk phenomena can be quantified and characterized with ease and with ensemble-representative reliability. With four shapes of NPs (Au spheres and Cu cubes, truncated octahedra and tetrahedra) and three Cu-based surface-alloy NPs (CuAg, CuPd and CuPdAg) as successful examples, we believe that the protocol can be applied to more complex structures and other inorganic nanomaterials in the future. We hope this method to find use in, amongst others, materials science, materials chemistry, (nano)physics, (nano)photonics, catalysis and electrochemistry.

5. Methods

5.1 Chemicals

The following chemicals and solvents were acquired from Sigma-Aldrich: copper bromide 99.99% (CuBr), palladium chloride 99% ($PdCl_2$), nitric acid 70% (HNO_3), trioctylphosphine oxide 99% (TOPO), trioctylphsopshine 99% (TOP), oleyl amine 70% (OLAM), polyvinylpyrrolidone (PVP, MW ~55,000), dichloromethane (DCM), and dimethyl formamide (DMF). Anhydrous ethanol 95% was purchased from ACROS organics (EtOH) and anhydrous toluene (99.8%) from Alfa Asear. Silver nitrate 99.9995% was obtained from Puratrem ($AgNO_3$). All chemicals were used as received without any further purification. All aqueous solutions were prepared with di-ionized (DI) water with a resistivity of 18.2 MΩ cm^{-1}.

5.2 Synthesis of anisotropic copper crystals

Cu NPs of three different morphologies were synthesized using a reflux set-up under inert conditions. For the C-Cu synthesis, adapted from Guo et al and Loiudice et al,[49,50] 0.45904 g CuBr and 1.78 mL TOP stored in a glove box, were mixed with 9 mL of degassed OLAM and sonicated for 10 min to form a transparent, pale yellow solution. Meanwhile, 50 mL of OLAM (70 %) were added to a 250 mL three-necked flask and degassed under vacuum. The flask was purged with N_2 after the bubble formation has stopped. Using a clean syringe, the reaction

mixture was then quickly added to the flask. The mixture was heated to 80 ºC using a heating mantle and kept at that temperature for 30 min while using a low vacuum to dry the solution. The yellow transparent reaction mixture was purged with N_2 and the temperature was quickly increased to 270 ºC and kept for 1 hour. At 270 ºC, the reaction mixture turned red, indicating nucleation. After the solution had cooled to room temperature, the reaction mixture was transferred to the glove box and washed with toluene using centrifugation (7,500 rpm for 5 min). The C-Cu pellet was redispersed in 5 mL of toluene. For TOh-Cu, the reaction was carried out at 260 ºC instead, all other conditions were kept the same. For the Th-Cu, 0.23908 g CuBr and 3.12417 g dry TOPO were dissolved in 5 mL degassed OLAM using ultrasonication (10 min), yielding a pale-yellow translucent solution. This was then quickly added to 34 mL OLAM in a three-necked flask under inert atmosphere using a syringe. Then, the temperature was raised to 80 ºC under vacuum, kept for 30 min, and raised further to 180 ºC to cause boiling. The pale-yellow solution turned to a deep gold color. At this point, a N_2 purge was applied and the temperature was further raised to 260 ºC upon which the solution turned translucent black, indicating nucleation. The reaction was continued for 1 h to yield a purple dispersion, which was then washed using toluene.

5.3 Synthesis of multimetallic NPs

The synthesis of the multimetallic NPs was inspired by the protocol from Lee et al.[51] 4 mg of NPs dispersed in toluene were added to a 10 mL glass vial to which 3.5 mL of degassed OLAM were carefully added, without disturbing the NP film. Additionally, 0.5 mg of dry $AgNO_3$ or $PdCl_2$ were added to 1.5 mL of degassed OLAM and heated at 50 or 80 ºC using an oil bath until dissolved. $AgNO_3$ or $PdCl_2$ in OLAM was then carefully added to the reaction vial, which was then allowed to react at 80 ºC for 60 s with C-Cu and TOh-Cu, or 50 ºC for 300 s with Th-Cu, after which the reaction was quenched with toluene. This yielded the Th- and TOh-CuAg and C-CuAg/Pd. For the synthesis of C-CuPdAg, 4 mg of C-CuAg rather than C-Cu NPs were used instead. All other parameters were kept the same. The coated crystals were washed with toluene and stored in a glovebox.

5.4 Preparation of aqueous dispersions

100 μL of the (multi)metallic anisotropic nanoparticle dispersions at concentrations of 2-20 mg mL^{-1} were ligand exchanged by washing with DMF (1 mL, 5,000 rpm and 2 min) in three-fold and dispersed in 100 μL DMF using the protocol of Johnson et al.[52] An aliquot equivalent of

100,000 mL^{-1} over a 3-step dilution series was added to deionized water, which was used for sampling.[53,54]

5.5 Characterization

Electron microscopy (EM). LR-TEM images were acquired with a FEI Tecnai Basic Spirit operated at 120 kV in bright field mode. The microscope was equipped with a Gatan charge-coupled device (CCD) camera and Digital Micrograph for imaging. Samples were drop-casted on ultrathin 400 mesh carbon film Au grids from Ted Pella Inc., which were washed with ethanol before and after drop-casting. Size distributions were obtained through edge-length analysis using the FIJI ImageJ software package of at least 100 unique particles. Scanning transmission electron microscopy high-angle annular dark-field (STEM-HAADF) micrographs and EDX elemental maps were obtained using a FEI Tecnai Osiris operated at 200 kV. The high-resolution TEM is outfitted with a X-FEG field emission gun reaching a brightness of 1.8×10^9 A cm^{-2} srad at 200 kV and when operated in scanning mode optimized for EDX, has a probe size of 1.0 nm with a current of 1 nA. The silicon drift Super-X EDX detectors in combination with the Bruker Esprit imaging software were used to acquire and analyze the EDX elemental maps.

X-ray photoelectron spectroscopy (XPS). XPS was performed with a Kratos Axis Supra system, using a monochromated Al K$_\alpha$ (1486.61 eV) X-ray source at a nominal power of 225 W. The samples were drop-casted on gold foil in a N$_2$ glovebox and transferred for measurement without exposure to air. No charge compensation was required and the binding energies (BEs) were referenced to Au 4f$_{7/2}$ at 83.95 eV. A pass energy of 20 eV was used for acquiring all core-level and Auger electron spectra.

Inductively coupled plasma – optical emission spectroscopy (ICP-OES). The concentration of the NP solution was determined with an Agilent 5110 ICP-OES with a VistaChip II CCD camera. The NPs were digested overnight in 2% HNO$_3$ and filtered with 0.4 μm pore size Ultrapore nylon filters. The calibration curves were obtained through the preparation of a dilution series of elemental standards obtained from Sigma Aldrich.

Inductively-coupled plasma mass spectrometry (ICP-MS). Particle sizing, counting and elemental analysis of the C-, TOh- and Th-Cu NPs as well as C-, TOh- and Th-CuAg NSAs was achieved with a NexION 350D ICP-MS instrument from PerkinElmer operated in continuous data acquisition mode. An icpTOF instrument of TOFWERK AG, Thun, Switzerland equipped with an orthogonal-acceleration TOF mass analyzer was used to size C-

Cu and determine the composition of C-CuAg, C-CuPd, and C-CuPdAg NPs. For a comparison of the operating conditions of both ICP-MS instruments see **Table S6**. Particles were extracted from the raw data using both commercial software from Perkin Elmer (Syngistix) and TOFWERK AG (TofPilot) as well as via an in-house developed MATLAB script (see **Table S7**). In the case of Syngistix and our MATLAB script, data processing, e.g., particle event extraction, was achieved by averaging over all intensities (counts) and determining the standard deviation (σ). A particle event is defined as any intensity 3σ above the average of all intensity counts (raw data).[30,55] This is done iteratively. After the first set of particle events has been collected, which are all the intensities (counts) above the determined threshold, the average and the σ of the new data-set (remaining intensity counts) is determined and the process is repeated until no signal >average + 3σ remains. TofPilot performs iterative signal/background separation every 1000 data points instead.[56,57] This allows for corrections in fluctuations of the dissolved signal. The average and σ are determined for each data subset with the threshold of a particle event defined as >average + (3.29σ) + 2.72 reducing false positives. Alternative methods to reduce false positives exist as well, which may offer better results under certain conditions.[58,59] Calibration of the transport efficiency (η_t) of the NexION 350D ICP-MS instrument was achieved in parallel with Au NPs standards of 61, 78 and 98 nm purchased from NanoComposix as well as 30, 50 and 80 nm purchased from PerkinElmer at number concentration of ~50,000 mL^{-1} (**Figures S1** and **S2**, **Table S8**). After Au NPs standards introduction, the instrument was rinsed with 1% HCl for 30 s and 2% HNO$_3$ after Cu, CuAg, CuPd and CuPdAg NP sampling. After rinsing with acid, i.e., before sample introduction, the sampler was rinsed with DI water. Dissolved metal calibration curves were obtained from elemental standards purchased from Sigma Aldrich. For the icpTOF instrument, calibration was achieved using an online droplet calibration method with a microdroplet generator described by Hendriks et al.[54] Monodisperse microdroplets of Cu, Pd, and Ag were used as calibrants and introduced into the NP aerosol flow in calibration run. Construction of the composition distributions was achieved in-house (see **Note S2**). The most abundant mass was used in all cases but inspected for false positives using all other isotopes and their respective LODs (See **Table S9** and **S10** for the LODs of the quadrupole and time-of-flight based methods respectively). For complex media, or highly concentrated salts such as phosphate buffered saline (PBS), matrix effects, such as spectral overlap and intensity changes, may significantly affect sizing and or composition determination accuracy.[53,54] Since in the present study only aqueous dispersions were used, matrix effects were of lesser concern. Further, the calibration

method used in this work ensures that the analyte and calibrant experience the same plasma conditions, thus allowing for matrix-independent mass quantification.

Acknowledgement

Supporting Information

The Supporting Information is available free of charge at https://pubs.acs.org/doi/. Experimental details, additional data, derivation of the model, and figures of merit of the methods (Figures S1−S14, Tables S1−S10, and Note S1-5) (PDF).

6. References

(1) Liz-Marzán, L. M. Tailoring Surface Plasmons through the Morphology and Assembly of Metal Nanoparticles. *Langmuir* **2006**, *22*, 32–41.

(2) Xia, Y.; Xiong, Y.; Lim, B.; Skrabalak, S. E. Shape-Controlled Synthesis of Metal Nanocrystals: Simple Chemistry Meets Complex Physics? *Angew. Chem. Int. Ed.* **2009**, *48*, 60–103.

(3) Jones, M. R.; Osberg, K. D.; Macfarlane, R. J.; Langille, M. R.; Mirkin, C. A. Templated Techniques for the Synthesis and Assembly of Plasmonic Nanostructures. *Chem. Rev.* **2011**, *111*, 3736–3827.

(4) Chen, G.; Qiu, H.; Prasad, P. N.; Chen, X. Upconversion Nanoparticles: Design, Nanochemistry, and Applications in Theranostics. *Chem. Rev.* **2014**, *114*, 5161–5214.

(5) Kleijn, S. E. F.; Lai, S. C. S.; Koper, M. T. M.; Unwin, P. R. Electrochemistry of Nanoparticles. *Angew. Chem. Int. Ed.* **2014**, *53*, 3558–3586.

(6) Liu, L.; Corma, A. Metal Catalysts for Heterogeneous Catalysis: From Single Atoms to Nanoclusters and Nanoparticles. *Chem. Rev.* **2018**, *118*, 4981–5079.

(7) Van Aert, S.; Batenburg, K. J.; Rossell, M. D.; Erni, R.; Van Tendeloo, G. Three-Dimensional Atomic Imaging of Crystalline Nanoparticles. *Nature* **2011**, *470*, 374–377.

(8) Laramy, C. R.; Brown, K. A.; O'Brien, M. N.; Mirkin, Chad. A. High-Throughput, Algorithmic Determination of Nanoparticle Structure from Electron Microscopy Images. *ACS Nano* **2015**, *9*, 12488–12495.

(9) Lee, B.; Yoon, S.; Lee, J. W.; Kim, Y.; Chang, J.; Yun, J.; Ro, J. C.; Lee, J.-S.; Lee, J. H. Statistical Characterization of the Morphologies of Nanoparticles through Machine Learning Based Electron Microscopy Image Analysis. *ACS Nano* **2020**, *14*, 17125–17133.

(10) Chen, C.; Kang, Y.; Huo, Z.; Zhu, Z.; Huang, W.; Xin, H. L.; Snyder, J. D.; Li, D.; Herron, J. A.; Mavrikakis, M.; Chi, M.; More, K. L.; Li, Y.; Markovic, N. M.; Somorjai, G. A.; Yang, P.; Stamenkovic, V. R. Highly Crystalline Multimetallic Nanoframes with Three-Dimensional Electrocatalytic Surfaces. *Science* **2014**, *343*, 1339–1343.

(11)   Choukroun, D.; Pacquets, L.; Li, C.; Hoekx, S.; Arnouts, S.; Baert, K.; Hauffman, T.; Bals, S.; Breugelmans, T. Mapping Composition–Selectivity Relationships of Supported Sub-10 Nm Cu–Ag Nanocrystals for High-Rate CO2 Electroreduction. *ACS Nano* **2021**, *15*, 14858–14872.

(12)   *Particle Analysis*. ImageJ Wiki. https://imagej.github.io/imaging/particle-analysis (accessed 2021-09-21).

(13)   Mondini, S.; Ferretti, A. M.; Puglisi, A.; Ponti, A. PEBBLES and PEBBLEJUGGLER: Software for Accurate, Unbiased, and Fast Measurement and Analysis of Nanoparticle Morphology from Transmission Electron Microscopy (TEM) Micrographs. *Nanoscale* **2012**, *4*, 5356–5372.

(14)   Pace, H. E.; Rogers, N. J.; Jarolimek, C.; Coleman, V. A.; Higgins, C. P.; Ranville, J. F. Determining Transport Efficiency for the Purpose of Counting and Sizing Nanoparticles via Single Particle Inductively Coupled Plasma Mass Spectrometry. *Anal. Chem.* **2011**, *83*, 9361–9369.

(15)   Laborda, F.; Jiménez-Lamana, J.; Bolea, E.; Castillo, J. R. Selective Identification, Characterization and Determination of Dissolved Silver(I) and Silver Nanoparticles Based on Single Particle Detection by Inductively Coupled Plasma Mass Spectrometry. *J. Anal. At. Spectrom.* **2011**, *26*, 1362–1371.

(16)   Pace, H. E.; Rogers, N. J.; Jarolimek, C.; Coleman, V. A.; Higgins, C. P.; Ranville, J. F. Correction to Determining Transport Efficiency for the Purpose of Counting and Sizing Nanoparticles via Single Particle Inductively Coupled Plasma Mass Spectrometry. *Anal. Chem.* **2012**, *84*, 4633–4633.

(17)   Mitrano, D. M.; Lesher, E. K.; Bednar, A.; Monserud, J.; Higgins, C. P.; Ranville, J. F. Detecting Nanoparticulate Silver Using Single-Particle Inductively Coupled Plasma–Mass Spectrometry. *Environ. Toxicol. Chem.* **2012**, *31*, 115–121.

(18)   Borovinskaya, O.; Hattendorf, B.; Tanner, M.; Gschwind, S.; Günther, D. A Prototype of a New Inductively Coupled Plasma Time-of-Flight Mass Spectrometer Providing Temporally Resolved, Multi-Element Detection of Short Signals Generated by Single Particles and Droplets. *J. Anal. At. Spectrom.* **2013**, *28*, 226–233.

(19)   Vogl, J. Calibration Strategies and Quality Assurance. In *Inductively Coupled Plasma Mass Spectrometry Handbook*; S.M. Nelms (Ed.), Blackwell Publishing, Oxford UK, 2005; pp 147–181.

(20)   Mozhayeva, D.; Engelhard, C. A Critical Review of Single Particle Inductively Coupled Plasma Mass Spectrometry – A Step towards an Ideal Method for Nanomaterial Characterization. *J. Anal. At. Spectrom.* **2020**, *35*, 1740–1783.

(21)   Mitrano, D. M.; Barber, A.; Bednar, A.; Westerhoff, P.; Higgins, C. P.; Ranville, J. F. Silver Nanoparticle Characterization Using Single Particle ICP-MS (SP-ICP-MS) and Asymmetrical Flow Field Flow Fractionation ICP-MS (AF4-ICP-MS). *J. Anal. At. Spectrom.* **2012**, *27*, 1131–1142.

(22)   Liu, J.; Murphy, K. E.; MacCuspie, R. I.; Winchester, M. R. Capabilities of Single Particle Inductively Coupled Plasma Mass Spectrometry for the Size Measurement of Nanoparticles: A Case Study on Gold Nanoparticles. *Anal. Chem.* **2014**, *86*, 3405–3414.

(23)   Laborda, F.; Bolea, E.; Jiménez-Lamana, J. Single Particle Inductively Coupled Plasma Mass Spectrometry for the Analysis of Inorganic Engineered Nanoparticles in Environmental Samples. *Trends Environ. Anal. Chem.* **2016**, *9*, 15–23.

(24)   Hendriks, L.; Gundlach-Graham, A.; Günther, D. Analysis of Inorganic Nanoparticles by Single-Particle Inductively Coupled Plasma Time-of-Flight Mass Spectrometry. *Chim. Int. J. Chem.* **2018**, *72*, 221–226.

(25)   Hadioui, M.; Knapp, G.; Azimzada, A.; Jreije, I.; Frechette-Viens, L.; Wilkinson, K. J. Lowering the Size Detection Limits of Ag and TiO2 Nanoparticles by Single Particle ICP-MS. *Anal. Chem.* **2019**, *91*, 13275–13284.

(26)   Folens, K.; Van Acker, T.; Bolea-Fernandez, E.; Cornelis, G.; Vanhaecke, F.; Du Laing, G.; Rauch, S. Identification of Platinum Nanoparticles in Road Dust Leachate by Single Particle Inductively Coupled Plasma-Mass Spectrometry. *Sci. Total Environ.* **2018**, *615*, 849–856.

(27)   Hegetschweiler, A.; Borovinskaya, O.; Staudt, T.; Kraus, T. Single-Particle Mass Spectrometry of Titanium and Niobium Carbonitride Precipitates in Steels. *Anal. Chem.* **2019**, *91*, 943–950.

(28) Donahue, N. D.; Kanapilly, S.; Stephan, C.; Marlin, M. C.; Francek, E. R.; Haddad, M.; Guthridge, J.; Wilhelm, S. Quantifying Chemical Composition and Reaction Kinetics of Individual Colloidally Dispersed Nanoparticles. *Nano Lett.* **2022**, *22*, 294–301.

(29) Strenge, I.; Engelhard, C. Single Particle Inductively Coupled Plasma Mass Spectrometry: Investigating Nonlinear Response Observed in Pulse Counting Mode and Extending the Linear Dynamic Range by Compensating for Dead Time Related Count Losses on a Microsecond Timescale. *J. Anal. At. Spectrom.* **2020**, *35*, 84–99.

(30) Degueldre, C.; Favarger, P.-Y.; Wold, S. Gold Colloid Analysis by Inductively Coupled Plasma-Mass Spectrometry in a Single Particle Mode. *Anal. Chim. Acta* **2006**, *555*, 263–268.

(31) Ho, K.-S.; Lui, K.-O.; Lee, K.-H.; Chan, W.-T. Considerations of Particle Vaporization and Analyte Diffusion in Single-Particle Inductively Coupled Plasma-Mass Spectrometry. *Spectrochim. Acta Part B At. Spectrosc.* **2013**, *89*, 30–39.

(32) Laborda, F.; Gimenez-Ingalaturre, A. C.; Bolea, E.; Castillo, J. R. About Detectability and Limits of Detection in Single Particle Inductively Coupled Plasma Mass Spectrometry. *Spectrochim. Acta Part B At. Spectrosc.* **2020**, *169*, 105883.

(33) Lee, S.; Bi, X.; Reed, R. B.; Ranville, J. F.; Herckes, P.; Westerhoff, P. Nanoparticle Size Detection Limits by Single Particle ICP-MS for 40 Elements. *Environ. Sci. Technol.* **2014**, *48*, 10291–10300.

(34) Shaw, P.; Donard, A. Nano-Particle Analysis Using Dwell Times between 10 Ms and 70 Ms with an Upper Counting Limit of Greater than 3 × 10 7 Cps and a Gold Nanoparticle Detection Limit of Less than 10 Nm Diameter. *J. Anal. At. Spectrom.* **2016**, *31*, 1234–1242.

(35) Reske, R.; Mistry, H.; Behafarid, F.; Roldan Cuenya, B.; Strasser, P. Particle Size Effects in the Catalytic Electroreduction of CO2 on Cu Nanoparticles. *J. Am. Chem. Soc.* **2014**, *136*, 6978–6986.

(36) Donahue, N. D.; Francek, E. R.; Kiyotake, E.; Thomas, E. E.; Yang, W.; Wang, L.; Detamore, M. S.; Wilhelm, S. Assessing Nanoparticle Colloidal Stability with Single-Particle Inductively Coupled Plasma Mass Spectrometry (SP-ICP-MS). *Anal. Bioanal. Chem.* **2020**, *412*, 5205–5216.

(37) Hou, Y.; Kovács, N.; Xu, H.; Sun, C.; Erni, R.; Gálvez-Vázquez, M. de J.; Rieder, A.; Hu, H.; Kong, Y.; Liu, M.; Wiley, B. J.; Vesztergom, S.; Broekmann, P. Limitations of Identical Location SEM as a Method of Degradation Studies on Surfactant Capped Nanoparticle Electrocatalysts. *J. Catal.* **2021**, *394*, 58–66.

(38) Holišová, V.; Urban, M.; Konvičková, Z.; Kolenčík, M.; Mančík, P.; Slabotinský, J.; Kratošová, G.; Plachá, D. Colloidal Stability of Phytosynthesised Gold Nanoparticles and Their Catalytic Effects for Nerve Agent Degradation. *Sci. Rep.* **2021**, *11*, 4071.

(39) Arena, D. A.; Bartynski, R. A.; Hulbert, S. L. The Electronic Structure of Ag/Cu(100) and Pd/Cu(100) Surface Alloys Studied by Auger-Photoelectron Coincidence Spectroscopy. In *Many-Particle Spectroscopy of Atoms, Molecules, Clusters, and Surfaces*; Berakdar, J., Kirschner, J., Eds.; Springer US: Boston, MA, 2001; pp 471–480.

(40) Merrifield, R. C.; Stephan, C.; Lead, J. R. Single-Particle Inductively Coupled Plasma Mass Spectroscopy Analysis of Size and Number Concentration in Mixtures of Monometallic and Bimetallic (Core-Shell) Nanoparticles. *Talanta* **2017**, *162*, 130–134.

(41) Praetorius, A.; Gundlach-Graham, A.; Goldberg, E.; Fabienke, W.; Navratilova, J.; Gondikas, A.; Kaegi, R.; Günther, D.; Hofmann, T.; Kammer, F. von der. Single-Particle Multi-Element Fingerprinting (SpMEF) Using Inductively-Coupled Plasma Time-of-Flight Mass Spectrometry (ICP-TOFMS) to Identify Engineered Nanoparticles against the Elevated Natural Background in Soils. *Environ. Sci. Nano* **2017**, *4*, 307–314.

(42) Naasz, S.; Weigel, S.; Borovinskaya, O.; Serva, A.; Cascio, C.; Undas, A. K.; Simeone, F. C.; Marvin, H. J. P.; Peters, R. J. B. Multi-Element Analysis of Single Nanoparticles by ICP-MS Using Quadrupole and Time-of-Flight Technologies. *J. Anal. At. Spectrom.* **2018**, *33*, 835–845.

(43) Ratuszek, M.; Zakrzewski, Z.; Majewski, J. Characteristics of Thermally Diffused Transit Areas of Single-Mode Telecommunication Fibers. *J. Light. Technol.* **2009**, *27*, 3050–3056.

(44) Demoulin, R.; Roussel, M.; Duguay, S.; Muller, D.; Mathiot, D.; Pareige, P.; Talbot, E. Atomic-Scale Characterization of N-Doped Si Nanocrystals Embedded in SiO2 by Atom Probe Tomography. *J. Phys. Chem. C* **2019**, *123*, 7381–7389.

(45) Perego, M.; Caruso, F.; Seguini, G.; Arduca, E.; Mantovan, R.; Sparnacci, K.; Laus, M. Doping of Silicon by Phosphorus End-Terminated Polymers: Drive-in and Activation of Dopants. *J. Mater. Chem. C* **2020**, *8*, 10229–10237.

(46) Hill, J. M.; Royce, D. G.; Fadley, C. S.; Wagner, L. F.; Grunthaner, F. J. Properties of Oxidized Silicon as Determined by Angular-Dependent X-Ray Photoelectron Spectroscopy. *Chem. Phys. Lett.* **1976**, *44*, 225–231.

(47) Löffler, T.; Savan, A.; Garzón-Manjón, A.; Meischein, M.; Scheu, C.; Ludwig, A.; Schuhmann, W. Toward a Paradigm Shift in Electrocatalysis Using Complex Solid Solution Nanoparticles. *ACS Energy Lett.* **2019**, *4*, 1206–1214.

(48) Hendriks, L.; Gundlach-Graham, A.; Hattendorf, B.; Günther, D. Characterization of a New ICP-TOFMS Instrument with Continuous and Discrete Introduction of Solutions. *J. Anal. At. Spectrom.* **2017**, *32*, 548–561.

(49) Guo, H.; Chen, Y.; Cortie, M. B.; Liu, X.; Xie, Q.; Wang, X.; Peng, D.-L. Shape-Selective Formation of Monodisperse Copper Nanospheres and Nanocubes via Disproportionation Reaction Route and Their Optical Properties. *J. Phys. Chem. C* **2014**, *118*, 9801–9808.

(50) Loiudice, A.; Lobaccaro, P.; Kamali, E. A.; Thao, T.; Huang, B. H.; Ager, J. W.; Buonsanti, R. Tailoring Copper Nanocrystals towards C2 Products in Electrochemical CO2 Reduction. *Angew. Chem. Int. Ed.* **2016**, *55*, 5789–5792.

(51) Lee, C.; Kim, N. R.; Koo, J.; Lee, Y. J.; Lee, H. M. Cu-Ag Core–Shell Nanoparticles with Enhanced Oxidation Stability for Printed Electronics. *Nanotechnology* **2015**, *26*, 455601.

(52) Johnson, N. J. J.; Sangeetha, N. M.; Boyer, J.-C.; Veggel, F. C. J. M. van. Facile Ligand-Exchange with Polyvinylpyrrolidone and Subsequent Silica Coating of Hydrophobic Upconverting β-NaYF4:Yb3+/Er3+ Nanoparticles. *Nanoscale* **2010**, *2*, 771–777.

(53) Tan, S. H.; Horlick, G. Matrix-Effect Observations in Inductively Coupled Plasma Mass Spectrometry. *J. Anal. At. Spectrom.* **1987**, *2*, 745–763.

(54) Hendriks, L.; Ramkorun-Schmidt, B.; Gundlach-Graham, A.; Koch, J.; Grass, R. N.; Jakubowski, N.; Günther, D. Single-Particle ICP-MS with Online Microdroplet Calibration: Toward Matrix Independent Nanoparticle Sizing. *J. Anal. At. Spectrom.* **2019**, *34*, 716–728.

(55) Degueldre, C.; Favarger, P.-Y.; Rossé, R.; Wold, S. Uranium Colloid Analysis by Single Particle Inductively Coupled Plasma-Mass Spectrometry. *Talanta* **2006**, *68*, 623–628.

(56) Gschwind, S.; Flamigni, L.; Koch, J.; Borovinskaya, O.; Groh, S.; Niemax, K.; Günther, D. Capabilities of Inductively Coupled Plasma Mass Spectrometry for the Detection of Nanoparticles Carried by Monodisperse Microdroplets. *J. Anal. At. Spectrom.* **2011**, *26*, 1166–1174.

(57) Ramkorun-Schmidt, B.; Pergantis, S. A.; Esteban-Fernández, D.; Jakubowski, N.; Günther, D. Investigation of a Combined Microdroplet Generator and Pneumatic Nebulization System for Quantitative Determination of Metal-Containing Nanoparticles Using ICPMS. *Anal. Chem.* **2015**, *87*, 8687–8694.

(58) Tuoriniemi, J.; Cornelis, G.; Hassellöv, M. A New Peak Recognition Algorithm for Detection of Ultra-Small Nano-Particles by Single Particle ICP-MS Using Rapid Time Resolved Data Acquisition on a Sector-Field Mass Spectrometer. *J. Anal. At. Spectrom.* **2015**, *30*, 1723–1729.

(59) Laborda, F.; Gimenez-Ingalaturre, A. C.; Bolea, E.; Castillo, J. R. Single Particle Inductively Coupled Plasma Mass Spectrometry as Screening Tool for Detection of Particles. *Spectrochim. Acta Part B At. Spectrosc.* **2019**, *159*, 105654.

Table of contents